nature nanotechnology

ARTICLES

https://doi.org/10.1038/s41565-019-0383-4

Emission and propagation of 1D and 2D spin waves with nanoscale wavelengths in anisotropic spin textures

Volker Sluka[1*], Tobias Schneider[1], Rodolfo A. Gallardo[2,3], Attila Kákay[1], Markus Weigand[4], Tobias Warnatz[1,10], Roland Mattheis[5], Alejandro Roldán-Molina[6], Pedro Landeros[2,3], Vasil Tiberkevich[7], Andrei Slavin[7], Gisela Schütz[4], Artur Erbe[1], Alina Deac[1], Jürgen Lindner[1], Jörg Raabe[8], Jürgen Fassbender[1,9] and Sebastian Wintz[1,8*]

Spin waves offer intriguing perspectives for computing and signal processing, because their damping can be lower than the ohmic losses in conventional complementary metal–oxide–semiconductor (CMOS) circuits. Magnetic domain walls show considerable potential as magnonic waveguides for on-chip control of the spatial extent and propagation of spin waves. However, low-loss guidance of spin waves with nanoscale wavelengths and around angled tracks remains to be shown. Here, we demonstrate spin wave control using natural anisotropic features of magnetic order in an interlayer exchange-coupled ferromagnetic bilayer. We employ scanning transmission X-ray microscopy to image the generation of spin waves and their propagation across distances exceeding multiples of the wavelength. Spin waves propagate in extended planar geometries as well as along straight or curved one-dimensional domain walls. We observe wavelengths between 1 µm and 150 nm, with excitation frequencies ranging from 250 MHz to 3 GHz. Our results show routes towards the practical implementation of magnonic waveguides in the form of domain walls in future spin wave logic and computational circuits.

Spin waves, also referred to as magnons, are the elementary excitations of the order parameter in ferromagnetic materials (Fig. 1a)[1]. They can be used in a similar manner to electrons in CMOS circuitry to transmit information, but with lower losses. Therefore, they are currently attracting a lot of interest as possible information carriers in alternative computing schemes[2–5]. Another substantial advantage of spin wave technology is the fact that, in the gigahertz range, magnon wavelengths are several orders of magnitude shorter than those of electromagnetic waves[6]. Accordingly, significant device miniaturization can be achieved for applications where the wavelength imposes a critical constraint on the device footprint. For such purposes it will be crucial to utilise spin waves with wavelengths in the submicrometre range, where both magnetostatic and exchange effects are relevant (dipole-exchange waves)[3]. While surface acoustic waves are already present as short-wavelength signal carriers in today's communication technology, spin waves offer a superior scalability of wave excitation and propagation at frequencies above 2 GHz as well as a much wider frequency tunability[7,8].

Two challenging aspects of building a magnonic computer are the generation of short-wavelength magnons[9–17] and the construction of suitable waveguides for spin wave transport[17–25]. A standard method to coherently generate spin waves employs the localized Oersted fields from alternating electric currents flowing in metallic antennas that are patterned adjacent to a magnetic medium. The smallest excitable wavelengths that are possible using this method, however, are approximately equal to the patterning sizes involved (Supplementary Section 3). In terms of nanopatterning and microwave impedance matching, it is therefore highly challenging to efficiently scale such an antenna-based excitation to nanoscale wavelengths. While similar restrictions apply from the patterning size, spin-transfer torques are an alternative suitable source for spin wave excitation[26–29], with the possibility of steering spin waves with external magnetic bias fields[29]. More recently, it has also been shown that spin waves can be generated using the internal fields of non-uniform spin textures[11–16,30–33], yet direct observations are limited to wavelengths >1 µm, apart from those in refs. [17,34,35]. Reference [34] demonstrates the emission of high-amplitude nanoscale spin waves from a pair of stacked vortex cores[36] driven by an alternating magnetic field[37,38]. However, in the geometry of ref. [34], where a point-like vortex core source is radiating spin waves into a two-dimensional (2D) propagation medium, spin waves originating from a vortex core and travelling outwards radially experience not only Gilbert damping, but also a purely geometric reduction of amplitude proportional to the inverse square root of the distance from the source, as shown schematically in Fig. 1b. Furthermore, it has been suggested that magnetic domain walls could be harnessed to guide spin waves across the magnonic chip[5,17–21,39–41]. In particular, it has been shown that domain walls can host localized modes excited by alternating magnetic fields[19]. In ref. [19], the lateral position of the excited magnetization amplitudes could be well controlled by tuning the lateral domain wall position, but these modes quickly decayed

[1]Helmholtz-Zentrum Dresden-Rossendorf, Dresden, Germany. [2]Universidad Técnica Federico Santa María, Valparaíso, Chile. [3]Center for the Development of Nanoscience and Nanotechnology (CEDENNA), Santiago, Chile. [4]Max-Planck-Institut für Intelligente Systeme, Stuttgart, Germany. [5]Leibniz Institut für Photonische Technologien, Jena, Germany. [6]Universidad de Aysén, Coyhaique, Chile. [7]Oakland University, Rochester, MI, USA. [8]Paul Scherrer Institut, Villigen, PSI, Switzerland. [9]Technische Universität Dresden, Dresden, Germany. [10]Present address: Uppsala Universitet, Uppsala, Sweden.
*e-mail: v.sluka@hzdr.de; s.wintz@hzdr.de

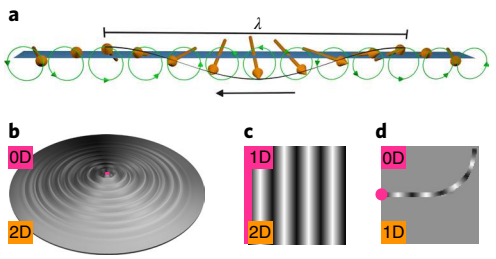

Fig. 1 | Spin waves in different geometries. a, Schematic of a spin wave of wavelength λ propagating along the direction indicated by the black arrow. The green arrows refer to the precessional motion performed by the magnetization vectors (orange arrows). **b**–**d**, Three different geometries of spin wave propagation explored in this Article. The magenta and orange fields denote the geometric dimensions of the source and propagation medium, respectively. In **b**, spin wave emission is from a point source. In this case, the dimensions of the medium and source differ by two. As a result, in addition to the exponential decay caused by Gilbert damping, there is a geometric decay of the spin wave amplitude. In **c**, plane-wave-like spin wave propagation is shown. Similar to **b**, the waveguide medium is 2D, yet the source has dimension one. In **d**, a 0D source excites a 1D medium (a domain wall).

along the domain wall coordinate with increasing distance from the microwave antenna within subwavelength length scales.

These key issues—short-wavelength spin wave generation and spin wave guidance—are the points we address in this work, where we make use of naturally formed anisotropic spin textures. First, we demonstrate the excitation and propagation of 2D planar spin waves (Fig. 1c) excited by the oscillation of straight domain walls. These excitations can travel distances spanning multiples of the wavelength. Second, we observe excitation and propagation of spin wave modes confined to quasi-1D natural waveguides (straight or curved) formed by domain walls embedded in a 2D host medium (Fig. 1d).

Anisotropic spin textures

We patterned $Ni_{81}Fe_{19}$/Ru/$Co_{40}Fe_{40}B_{20}$ multilayers (44.9/0.8/46.6 nm thickness) into disk- and square-shaped elements with lateral sizes of several micrometres (Fig. 2a). Each ferromagnetic layer exhibits an in-plane uniaxial anisotropy. The Ru interlayer causes antiferromagnetic coupling between the two ferromagnetic layers[42] (see Methods for further details).

The magnetic ground-state configuration stabilized in this system is a pair of stacked vortices, with opposite vorticity due to the antiferromagnetic interlayer exchange coupling. The influence of the CoFeB uniaxial anisotropy leads to a significant distortion of the vortex magnetization distribution in both magnetic layers. The result in each layer is a state of two homogeneously in-plane magnetized domains with opposite magnetizations. These domains are separated by a narrow, partially perpendicularly oriented, 180° domain wall that contains the vortex cores and spans the lateral extension of the disks. These magnetic configurations are presented in the scanning transmission X-ray microscopy (STXM) images in Fig. 2b,c, which display magnetic information about the in-plane (Fig. 2b) and out-of plane (Fig. 2c) components of the individual layers, where the technique provides a lateral resolution of about 25 nm. As Fig. 2c indicates, the out-of-plane magnetization components of the respective layers couple ferromagnetically to each other via their stray field. In particular, this is true for the polarizations of the vortex cores. Micromagnetic simulations confirm this and reveal that the domain wall formed in the sample is a mixture of Néel and Bloch types of domain wall[43], where the in-plane components couple antiferromagnetically across the Ru interlayer, as in the domains. Figure 2d presents a schematic top view of the domain wall structure in the CoFeB layer, showing the mixed Bloch and Néel components. Figure 2e shows a schematic cross-section across the domain wall, revealing that the out-of-plane magnetization components in the domain wall follow a flux-closing distribution between the two layers.

Nanoscale spin wave generation

Spin waves can be excited in such anisotropic spin textures by applying an alternating magnetic field, as shown in Fig. 3. The corresponding measurements were made by means of time-resolved (TR) STXM imaging, allowing for a stroboscopic time resolution of ~100 ps. Figure 3a presents a snapshot of the magnetic excitations at an Oersted field frequency of 1.11 GHz, taken at the Ni absorption edge, displaying the out-of-plane contrast. Plane spin waves are visible, with wave fronts parallel to the domain wall and propagating away from the domain wall towards the rim of the elliptical element, as indicated by the green arrow. The oscillating Oersted-field in-plane component is oriented along the minor axis of the ellipse, perpendicular to the domain wall. The main effect of the Oersted field is to excite the dynamics of the domain wall, and the excited domain wall acts as a confined perpendicular source for the observed spin waves[15,17,33]. In more detail, by acting on the full sample volume, the field excites a non-resonant antiphase width oscillation of the walls in the two different layers, which is coherent over the wall length, causing highly localized out-of-plane torques in the wall vicinity. In this way, spin waves are essentially excited via a linear and coherent coupling of the discrete wall mode to the spin wave continuum, similar to the situation with vortex core-driven spin waves, as reported earlier[34,35].

The time-periodic nature of the waves allows us to capture the wave motion at discrete, equi-spaced phases in each scanned pixel, and to compose the recorded data into movie-like arrangements, which show the propagation of these spin excitations (see videos in the Supplementary Information). A comparison of the absorption data taken along the green arrow in Fig. 3a at different time slices yields the wavelength of the wave and its speed of propagation. Three of these time slices are shown in Fig. 3b. Notably, the spin wave amplitude does not visibly decrease across the distance of 2 µm, corresponding to about 7.5 times the wavelength. Taking into account a set of measurements for the given frequency of 1.11 GHz, we obtain a wavelength of 286 ± 20 nm and a phase velocity of 317 ± 22 m s^{-1}. Increasing the excitation frequency to 1.46 GHz results in a similar wave pattern, but with shorter wavelength (Fig. 3c). The corresponding values for the wavelength and phase velocity are 211 ± 15 nm and 307 ± 22 m s^{-1}, respectively. By comparison with the contrast of the vortex core, the spin wave amplitudes are estimated to reach a precession angle of more than 5°, which can be considered as very high when compared to standard spin wave excitation techniques (cf. ref. [44], which reports an angle of 1.5°).

Around the vortex centre, as shown in the magnified image in Fig. 3d, in addition to the plane waves generated by the oscillating wall, there are radial wave fronts that arise from the motion of the vortex core[34]. As expected, these radially symmetric waves decay faster than the plane waves excited by the domain wall. This difference is a consequence of the relative dimensionality of the source and medium: while the plane waves are excited by a 1D source (the domain wall), for the radial waves the source is 0D (the vortex core). Nevertheless, as the two wave forms are excited simultaneously, interference patterns arise (Fig. 3d).

We can excite planar spin waves for a broad range of frequencies up to 3 GHz. One can expect this process to scale to higher frequencies if the magnetization gradient of the exciting source (domain wall or vortex core) is enhanced as for domain walls in systems with strong perpendicular magnetic anisotropy or if the spin wave dispersion relation is tuned to longer wavelengths by modifying

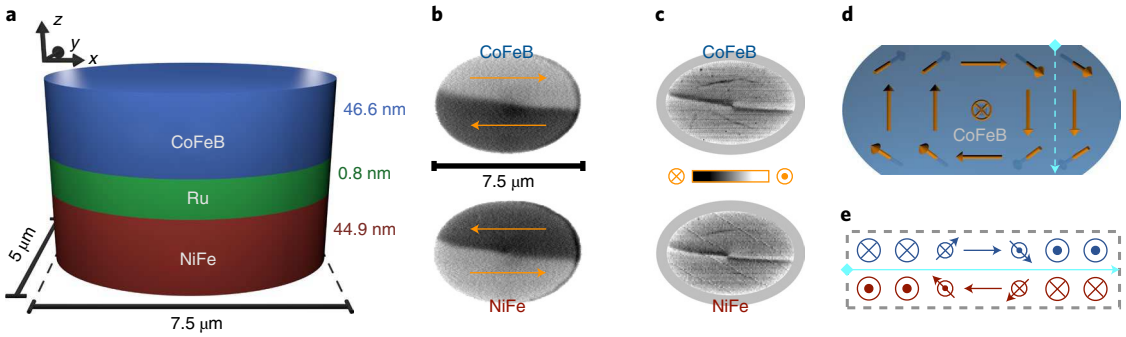

Fig. 2 | Sample layout and magnetic configuration. a, The ferromagnetic element is patterned out of an interlayer-exchange-coupled bilayer system consisting of a NiFe layer and a CoFeB layer, coupled antiferromagnetically by a Ru interlayer. **b**,**c**, High-resolution X-ray magnetic circular dichroism (XMCD) STXM images, showing that the magnetic configuration is a pair of stacked vortices, with antiferromagnetically coupled in-plane magnetizations. In **b**, the contrast represents the in-plane magnetic component along the long axis of the elliptic element (orange arrows indicate the magnetic orientation). In **c**, the out-of-plane magnetic contrast is displayed. We find that an additional anisotropy with the easy axis along the long axis of the elliptic element leads to an anisotropic deformation of the vortex patterns, resulting in the formation of a domain wall, which is also visible both in the in-plane and out-of-plane contrast images. Micromagnetic simulations reveal that this domain wall has both Néel and Bloch character, as shown schematically in **d**, where the orange arrows indicate the magnetic orientation. **e**, Cross-section of the domain wall profile, which can be imagined as taken along the blue dashed line in **d**, illustrating the in- and out-of-plane components of the layer magnetizations in and around the domain wall.

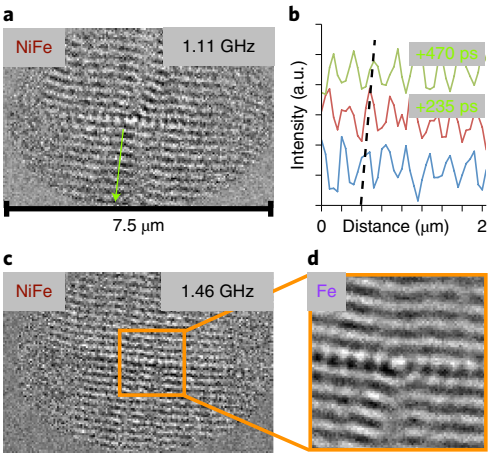

Fig. 3 | Excitation of spin waves. TR-STXM snapshots of spin waves (NiFe layer out-of-plane magnetization component), excited using a.c. magnetic fields at different frequencies. **a**, Spin waves generated at an excitation frequency of 1.11 GHz. These plane waves travel from the wall to the rim of the disk, as indicated by the green arrow. **b**, Three time slices of the signal amplitude along the arrow in **a** taken at equidistant time intervals of 235 ps. **c**, Corresponding image of a spin wave excited at 1.46 GHz. **d**, Enlarged image of the region indicated in the centre of **c**.

the magnetic layer stack. A qualitatively different effect, however, appears when going to rather low excitation frequencies, as shown in Fig. 4, which displays excitations at 0.52 GHz and 0.26 GHz (Fig. 4a,b, respectively). At these low frequencies, no visible excitations exist in the domains, yet the data show spin waves propagating confined to the domain wall in the directions away from the vortex cores. The wavelength can again be controlled by tuning the excitation frequency. Note that there is a directional asymmetry in the spin wave emission at 0.52 GHz, which, however, can be attributed to sample imperfections in the exciting core region, as simulations indicate a symmetric emission pattern (Supplementary Video 7). Irrespective of this, the wave amplitude is still significant, even after a propagation distance extending from the vortex core to the rim of the ellipse. This situation is again a consequence of a dimensionality difference of one between source and medium. For waves propagating along the domain wall, the source is of dimension zero, yet the propagation medium is effectively 1D. Hence, geometrical decay of the amplitude is avoided, making the domain wall act as a low-loss waveguide (Supplementary Video 4) of propagating spin waves in the domain walls. The confined waves excited here can be considered a bilayer analogue of the spin wave mode predicted for a single domain wall[40]. The coherent domain wall resonance (or infinite wavelength $k=0$) case of such a bilayer has been theoretically studied[45] (cf. Supplementary Section 2).

To shed light on the underlying physics, we followed a twofold strategy. First, both phenomena—the excitation and propagation of planar spin waves in the domain and 1D waves confined to the domain wall—were investigated and qualitatively confirmed with micromagnetic simulations. To achieve this, the experimental static magnetization distribution was reproduced before excitation by an a.c. magnetic field. Supplementary Video 7 shows the time-dependent perpendicular magnetization of a simulated ellipse yielding a qualitative confirmation of the gapless 1D spin wave mode in the domain wall. To obtain details of the dispersion relation for the planar waves in the domains within a reasonable computation time, the system was modelled by two continuous, homogeneously magnetized coupled layers (see Methods for further details).

2D plane spin wave dispersion

In addition to the simulations, we developed a theory (see Supplementary Information for in-depth technical details) for the propagation of spin waves in two exchange-coupled extended ferromagnetic films. The theory allows to compute the spin wave dispersion relation in coupled films whose thicknesses exceed the respective material's exchange length. This is done by considering each magnetic layer as being composed of several coupled thin layers, for which the thin film approximation holds (for details see Methods). In Fig. 5, the measured spin wave dispersion relations $f(k=2\pi/\lambda)$ (where f denotes frequency, k is the wavenumber and λ is the wavelength) for waves in the domains and in the domain walls are combined with the analytical and micromagnetic simulation results. We first consider the planar waves propagating through the domains. The theoretical result is found to depend sensitively on the CoFeB in-plane uniaxial anisotropy K_u(CoFeB) and the interlayer exchange coupling J. For $J=-0.1\,\mathrm{mJ\,m^{-2}}$ and $K_u(\mathrm{CoFeB})=3\,\mathrm{kJ\,m^{-3}}$, we find good agreement with the experimental data. The elevated value of K_u(CoFeB) is reasonable, because

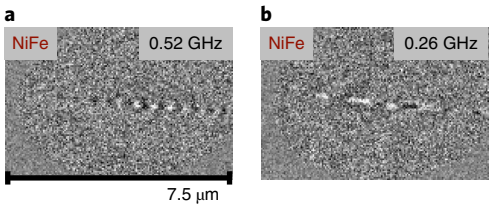

Fig. 4 | Spin waves in the domain wall. a,**b**, Spin waves confined to the domain wall (TR-STXM of the NiFe layer magnetization out-of-plane component) excited at 0.52 and 0.26 GHz, respectively, with accordingly changing wavelengths.

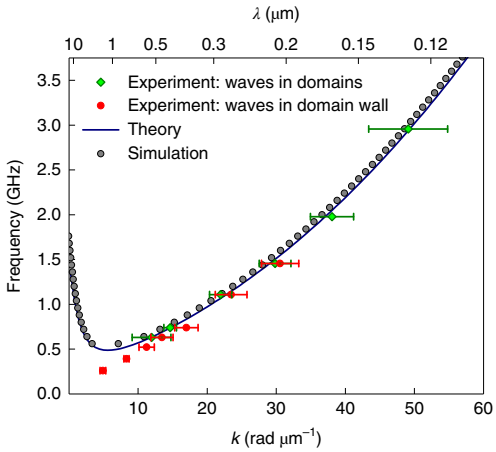

Fig. 5 | Spin wave dispersion relations. From the experiment, we obtain the dispersion relations for spin waves propagating in the domains (full green diamonds) and waves confined to the domain wall (red dots) with wavevectors $k = 2\pi/\lambda$. The error bars correspond to the uncertainty in the wavelength determination. In addition, we show the plane wave dispersions calculated using our model (blue continuous line) and micromagnetic simulations (grey dots), which are in good agreement.

we expect the CoFeB to react sensitively to strain exerted by the patterned waveguide microstructure onto the elliptical element[46]. Using the same parameters as in the theory, we also computed the dispersion using micromagnetic simulations (grey dots in Fig. 5), which were found to quantitatively reproduce the results from both the experiment and analytic calculations. Note that the antiparallel bilayer system considered here can in principle host two separate spin wave modes of acoustic and optical character (Supplementary Section 2). However, because the optical mode resides at much higher frequencies and is not accessed by our experiments, we only consider the acoustic mode in the following.

A striking feature of the acoustic plane wave dispersion is the existence of a local minimum at low k around 5 rad μm^{-1} and, accordingly, a frequency gap, below which no spin wave excitations are possible. The local minimum at some finite value of the wavevector in Fig. 5 results from a combination of the non-reciprocity induced by the dipolar coupling between the two antiferromagnetically coupled magnetic layers[34,47] (Supplementary Section 2) and the uniaxial magnetic anisotropy. Namely, when the anisotropy is zero, the collective dispersion in Damon–Eshbach geometry ($\mathbf{k}\perp\mathbf{M}_0$)[48] has a minimum of zero frequency at $k=0$, while at finite anisotropies this minimum is shifted to finite values of both wavevector and frequency. Such k-shifting of the dispersion minimum is somewhat analogous to that induced by the Dzyaloshinskii–Moriya interaction, for example for ferromagnetic–heavy metal interfaces, where the minimum of the dispersion is also shifted[49]. Note that we only observe the slow branch ($k \geq +5$ rad μm^{-1}) of the non-reciprocal dispersion relation in our experiment because the wavelengths of the fast branch waves for the given frequencies are of the order of the sample size or even exceed it (cf. Supplementary Section 2). At the same time the spin wave amplitudes predicted for the fast branch are much lower. Hence, spin wave edge reflections are not noticeable in the experiment.

1D spin waves along domain walls

Our experimental observations of selective excitation and propagation of spin waves in the domain wall can be explained based on the existence of the frequency gap discussed above. The red circles in Fig. 5 display the dispersion relation of the measured spin waves in the domain wall. In contrast to the planar waves in the domains, the waves confined to the wall exhibit an almost linear dispersion, which runs below its plane wave counterpart and, when extrapolated towards zero, intercepts the y axis close to $f=0$. Thus, when tuning the excitation frequency to values inside the gap, no propagating magnons are excited in the domains, and only the energetically lower modes existing in the wall are populated. The existence or absence of a gap in the domain and domain wall, respectively, are explained by the Goldstone theorem[50], which states that a system exhibiting a continuous symmetry spontaneously broken by the ground state has a gapless mode. In the case of spin waves in the domains, the corresponding system comprises the two coupled disks. Here, the continuous symmetry is compromised by the uniaxial anisotropy and, accordingly, the planar spin wave dispersion relation exhibits a gap. In the case of the waves confined to the domain wall, there exists a continuous translational symmetry that gives rise to a gapless mode. The presence of defects and the finite size of the sample, in principle, break this symmetry, but the resulting gap is too small to be observed in the experiment.

The idea of using domain walls as waveguides is intriguing, and Fig. 6 shows that the above described phenomenon indeed extends to cases where the walls are curved, that is, lead 'around the corner'. Neither is the concept restricted to continuous wave excitation. Figure 6a displays the static magnetization configuration (out-of-plane contrast) of a domain wall of the same type as above, but curved towards the right-hand rim of the magnetic element. Figure 6b–d displays snapshots of the excitation following a field pulse. Due to the width of the spectral composition of the pulse, spin waves are excited inside and above the frequency gap. The resulting plane wavepacket traverses the domains in the direction away from the wall and makes it easy to optically distinguish the domain wall wave from the remainder of the excitations. At 11.1 ns after the pulse, the wall wavepacket has reached the region in front of the turn (Fig. 6c); 2.5 ns later the wavepacket has travelled around the corner. Remarkably, even after the turn, the wavepacket maintains a detectable amplitude. While the spatial distribution of the domain wall in our experiment is solely a consequence of both dipolar sample confinement fields and magnetostrictive anisotropies, it was shown that further control of the domain wall position can be achieved, for example by exchange bias patterning[20,24], ferroelectric coupling[13,32] or external magnetic fields[19].

Conclusions

We have addressed several key aspects of magnonic computing by exploiting magnetic anisotropy. The first aspect is related to energy and the signal range. We have demonstrated that textures in a magnetization distribution, like domain walls and vortex cores, can serve as sources for the generation of short-wavelength, dipole-exchange spin waves of a directional nature, that is, planar waves in magnetic domains and waves confined to domain walls. These are, due to their geometry, not subject to a reduction of amplitude

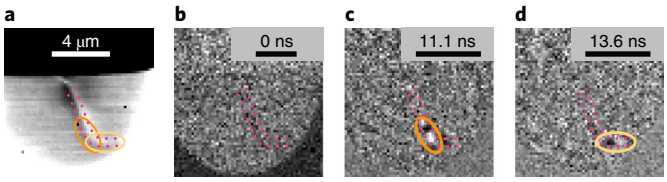

Fig. 6 | Domain walls as waveguides. We demonstrate the possibility of harnessing domain walls as waveguides for magnonic excitations by sending a spin wavepacket around a domain wall curving around a corner (TR-STXM images). **a**, An out-of-plane magnetic contrast image of the domain wall, with the position of the wall outlined by the red dotted line. Orange and yellow ellipses mark two regions in front and behind the curve, respectively. **b**–**d**, Snapshots of a spin wavepacket excited by a magnetic field pulse, at different times after the pulse. At 11.1 ns after the pulse (**c**), the wavepacket has reached the region in front of the curve. At 13.6 ns (**d**), the wavepacket has travelled around the corner.

due to the geometric dilution of the energy flow. Such waves minimize the losses occurring during propagation. Indeed, we found that the resulting excitations can travel distances easily spanning several micrometres, that is, significantly exceeding multiples of the nanoscale wavelengths—a necessary condition, for example, for magnon interference-based applications. The second aspect is to identify possible waveguides for magnonic chips. Here, we have shown that domain walls can serve as such waveguides, combining several useful properties. First, due to their inherent symmetry, and consequently their near-gapless dispersion relation, spin waves can be excited selectively in these structures. In addition, we have shown that spin wavepackets can travel along angled domain walls while largely maintaining their amplitude. Such a possibility of angled signal guidance is vital for chip design, and therefore our result may enable new solutions to the development of magnonic circuits.

Online content

Any methods, additional references, Nature Research reporting summaries, source data, statements of data availability and associated accession codes are available at https://doi.org/10.1038/s41565-019-0383-4.

Received: 2 August 2018; Accepted: 21 January 2019;
Published online: 25 February 2019

References

1. Bloch, F. Zur theorie des ferromagnetismus. *Z. Phys.* **61**, 206–209 (1930).
2. Kruglyak, V. V., Demokritov, S. O. & Grundler, D. Magnonics. *J. Phys. D* **43**, 264001 (2010).
3. Chumak, A. V., Serga, A. A. & Hillebrands, B. Magnon transistor for all-magnon data processing. *Nat. Commun.* **5**, 4700 (2014).
4. Chumak, A. V., Vasyuchka, V. I., Serga, A. A. & Hillebrands, B. Magnon spintronics. *Nat. Phys.* **11**, 453–461 (2015).
5. Lan, J., Yu, W., Wu, R. & Xiao, J. Spin-wave diode. *Phys. Rev. X* **5**, 041049 (2015).
6. Gurevich, A. G. & Melkov, G. A. *Magnetization Oscillations and Waves* (CRC, New York, 1996).
7. Oliner, A. A. *Acoustic Surface Waves* (Springer, Berlin, 1978).
8. Morgan, D. R. Surface acoustic wave devices and applications: 1. Introductory review. *Ultrasonics* **11**, 121–131 (1973).
9. Lee, K.-S., Choi, S. & Kim, S.-K. Radiation of spin waves from magnetic vortex cores by their dynamic motion and annihilation processes. *Appl. Phys. Lett.* **87**, 192502 (2005).
10. Demokritov, S. O. et al. Bose–Einstein condensation of quasi-equilibirum magnons at room temperature under pumping. *Nature* **443**, 430–433 (2006).
11. Davies, C. S., Poimanov, V. D. & Kruglyak, V. V. Mapping the magnonic landscape in patterned magnetic structures. *Phys. Rev.* **96**, 094439 (2017).
12. Mozooni, B. & McCord, J. Direct observation of closure domain wall mediated spin waves. *Appl. Phys. Lett.* **107**, 042402 (2015).
13. Wiele, B. V., Hämäläinen, S. J., Baláz, P., Montoncello, F. & Dijken, S. V. Tunable short-wavelength spin wave excitation from pinned magnetic domain walls. *Sci. Rep.* **6**, 21330 (2016).
14. Whitehead, N. J., Horsley, S. A. R., Philbin, T. G., Kuchko, A. N. & Kruglyak, V. V. Theory of linear spin wave emission from a Bloch domain wall. *Phys. Rev. B* **96**, 064415 (2017).
15. Hermsdoerfer, S. J. et al. A spin-wave frequency doubler by domain wall oscillation. *Appl. Phys. Lett.* **94**, 223510 (2009).
16. Holländer, R. B., Müller, C., Schmalz, J., Gerken, M. & McCord, J. Magnetic domain walls as broadband spin wave and elastic magnetisation wave emitters. *Sci. Rep.* **8**, 13871 (2018).
17. Sluka, V *et al.*in Stacked topological spin textures as emitters for multidimensional spin wave modes. *IEEE International Magnetics Conference (INTERMAG)* https://doi.org/10.1109/INTMAG.2015.7157029 (IEEE, 2015).
18. Garcia-Sanchez, F. et al. Narrow magnonic waveguides based on domain walls. *Phys. Rev. Lett.* **114**, 247206 (2015).
19. Wagner, K. et al. Magnetic domain walls as reconfigurable spin-wave nanochannels. *Nat. Nanotechnol.* **11**, 432–436 (2016).
20. Albisetti, E. et al. Nanoscale spin-wave circuits based on engineered reconfigurable spin-textures. *Commun. Phys.* **1**, 56 (2018).
21. Aliev, F. G. et al. Localized domain-wall excitations in patterned magnetic dots probed by broadband ferromagnetic resonance. *Phys. Rev. B* **84**, 144406 (2011).
22. Vogt, K. et al. Realization of a spin-wave multiplexer. *Nat. Commun.* **5**, 3727 (2014).
23. Gruszecki, P., Kasprzak, M., Serebryannikov, A. E., Krawczyk, M. & Smigaj, W. Microwave excitation of spin wave beams in thin ferromagnetic films. *Sci. Rep.* **6**, 22367 (2016).
24. Albisetti, E. et al. Nanopatterning reconfigurable magnetic landscapes via thermally assisted scanning probe lithography. *Nat. Nanotechnol.* **11**, 545–551 (2016).
25. Haldar, A., Kumar, D. & Adeyeye, A. O. A reconfigurable waveguide for energy-efficient transmission and local manipulation of information in a nanomagnetic device. *Nat. Nanotechnol.* **11**, 437–443 (2016).
26. Demidov, V. E., Urazhdin, S. & Demokritov, S. O. Direct observation and mapping of spin waves emitted by spin–torque nano-oscillators. *Nat. Mater.* **9**, 984–988 (2010).
27. Madami, M. et al. Direct observation of a propagating spin wave induced by spin-transfer torque. *Nat. Nanotechnol.* **6**, 635–638 (2011).
28. Urazhdin, S. et al. Nanomagnetic devices based on the spin–transfer torque. *Nat. Nanotechnol.* **9**, 509–513 (2014).
29. Bonetti, S. et al. Direct observation and imaging of a spin-wave soliton with p-like symmetry. *Nat. Commun.* **6**, 8889 (2015).
30. Yu, H. et al. Omnidirectional spin-wave nanograting coupler. *Nat. Commun.* **4**, 2702 (2013).
31. Yu, H. et al. Approaching soft X-ray wavelengths in nanomagnet-based microwave technology. *Nat. Commun.* **7**, 11255 (2016).
32. Hämäläinen, S. J., Brandl, F., Franke, K. J. A., Grundler, D. & van Dijken, S. Tunable short-wavelength spin-wave emission and confinement in anisotropy-modulated multiferroic heterostructures. *Phys. Rev. Appl.* **8**, 014020 (2017).
33. Voto, M., Lopez-Diaz, L. & Martinez, E. Pinned domain wall oscillator as tunable direct current spin wave emitter. *Sci. Rep.* **7**, 13559 (2017).
34. Wintz, S. et al. Magnetic vortex cores as tunable spin wave emitters. *Nat. Nanotechnol.* **11**, 948–953 (2016).
35. Dieterle, G. et al. Coherent excitation of heterosymmetric spin waves with ultrashort wavelengths. Preprint at https://arxiv.org/abs/1712.00681 (2017).
36. Shinjo, T., Okuno, T., Hassdorf, R., Shigeto, K. & Ono, T. Magnetic vortex core observation in circular dots of permalloy. *Science* **289**, 930–932 (2000).
37. Thiele, A. A. Steady-state of motion of magnetic domains. *Phys. Rev. Lett.* **30**, 230 (1973).
38. Choe, S.-B. et al. Vortex core-driven magnetization dynamics. *Science* **304**, 420–422 (2004).
39. Xing, X. & Zhou, Y. Fiber optics for spin waves. *NPG Asia Mater.* **8**, e246 (2016).
40. Winter, J. M. Bloch wall excitation. Application to nuclear resonance in a Bloch wall. *Phys. Rev.* **124**, 452 (1961).
41. Stoll, H. et al. High-resolution imaging of fast magnetization dynamics in magnetic nanostructures. *Appl. Phys. Lett.* **84**, 3328 (2004).
42. Grünberg, P., Schreiber, R., Pang, Y., Brodsky, M. B. & Sowers, H. Layered magnetic structures: evidence for antiferromagnetic coupling of Fe layers across Cr interlayers. *Phys. Rev. Lett.* **57**, 2442 (1986).
43. Labrune, M. & Miltat, J. Wall structures in ferro/antiferromagnetic exchange-coupled bilayers: a numerical micromagnetic approach. *J. Magn. Magn. Mater.* **151**, 231–245 (1995).
44. Groß, F. et al. Nanoscale detection of spin wave deflection angles in permalloy. *Appl. Phys. Lett.* **114**, 012406 (2019).
45. Stamps, R. L., Carriço, A. S. & Wigen, P. E. Domain-wall resonance in exchange-coupled magnetic films. *Phys. Rev. B* **55**, 6473–6484 (1997).
46. Wang, D., Nordman, C., Qian, Z., Daughton, J. M. & Myers, J. Magnetostriction effect of amorphous CoFeB thin films and application in spin-dependent tunnel junctions. *J. Appl. Phys.* **97**, 10C906 (2005).

47. Grünberg, P. Magnetostatic spinwave modes of a heterogeneous ferromagnetic double layer. *J. Appl. Phys.* **52**, 6824–6829 (1981).
48. Damon, R. W. & Eshbach, J. R. Magnetostatic modes of a ferromagnetic slab. *J. Phys. Chem. Solids.* **19**, 308–320 (1961).
49. Cho, J. et al. Thickness dependence of the interfacial Dzyaloshinskii–Moriya interaction in inversion symmetry broken systems. *Nat. Commun.* **6**, 7635 (2015).
50. Goldstone, J., Salam, A. & Weinberg, S. Broken symmetries. *Phys. Rev.* **127**, 965–970 (1962).

Acknowledgements

The authors thank B. Sarafimov, B. Watts and M. Bechtel for experimental support at the STXM beamlines, as well as C. Fowley, K. Kirsch, B. Scheumann and C. Neisser for their help with sample fabrication. Most of the experiments were performed at the Maxymus endstation at BESSY2, HZB, Berlin, Germany. The authors thank HZB for the allocation of synchrotron radiation beamtime. Some experiments were performed at the PolLux endstation at SLS, PSI, Villigen, Switzerland. Pollux is financed by BMBF via contracts 05KS4WE1/6 and 05KS7WE1. Support by the Nanofabrication Facilities Rossendorf at IBC, HZDR, Dresden, Germany is gratefully acknowledged. V.S. and A.D. acknowledge funding from the Helmholtz Young Investigator Initiative under grant VH-N6-1048. R.A.G. acknowledges financial support from FONDECYT Iniciacion 11170736 and 1161403. A.R.M. acknowledges funding from FONDECYT 3170647; funding from the Basal Program for Centers of Excellence, grant FB0807 CEDENNA, CONICYT is also acknowledged. V.T. and A.S. acknowledge support from the US National Science Foundation under grants EFMA-1641989 and ECCS-1708982 and from the DARPA M3IC grant under contract no. W911-17-C-0031. S.W. acknowledges funding from the European Community's Seventh Framework Programme (FP7/2007-2013) under grant agreement no. 290605 (PSI-FELLOW/COFUND).

Author contributions

S.W. conceived the experiment. V.S., M.W. and S.W. performed the STXM measurements. V.S. and S.W. analysed the data. T.S., T.W., A.K. and S.W. conducted the micromagnetic simulations. R.A.G., A.R.M. and P.L. calculated the spin wave dispersion relation. R.M. and S.W. supervised sample preparation. V.S. and S.W. wrote the manuscript. All authors discussed the results and commented on the manuscript.

Competing interests

The authors declare no competing interests.

Additional information

Supplementary information is available for this paper at https://doi.org/10.1038/s41565-019-0383-4.

Reprints and permissions information is available at www.nature.com/reprints.

Correspondence and requests for materials should be addressed to V.S. or S.W.

Journal peer review information *Nature Nanotechnology* thanks Ferran Macià, Takuya Satoh and other anonymous reviewer(s) for their contribution to the peer review of this work.

Publisher's note: Springer Nature remains neutral with regard to jurisdictional claims in published maps and institutional affiliations.

Methods

Sample fabrication. $Ni_{81}Fe_{19}$/Ru/$Co_{40}Fe_{40}B_{20}$/Al multilayers were deposited by magnetron sputtering on X-ray transparent silicon nitride membrane substrates of 200 nm thickness. The 5-nm-thick Al layer is used as capping for oxidation protection. From transmission electron microscopy (TEM) measurements, the NiFe and CoFeB thicknesses were determined to be 44.9 and 46.6 nm, respectively. The two ferromagnetic layers are subject to antiferromagnetic interlayer exchange coupling, mediated by the Ru layer (0.8 nm nominal thickness)[42], as indicated by hard axis magnetization reversal measured by the magneto-optical Kerr effect (MOKE) on extended multilayer films[51]. MOKE measurements performed on corresponding single-layer films of NiFe and CoFeB showed that these films exhibit colinear uniaxial anisotropies. The respective values for NiFe and CoFeB are 0.2 kJ m^{-3} and 1.1 kJ m^{-3}. However, a significantly higher uniaxial anisotropy value for CoFeB of about 3 kJ m^{-3} is needed in order to reproduce the experimentally found static magnetization distribution by micromagnetic simulations.

This elevated value for the in-plane uniaxial anisotropy in CoFeB can be attributed to strain, which in our case is caused by the contact with the waveguide. In fact, CoFeB is known for its sensitivity to strain, and the orientation of the experimentally observed magnetic pattern with respect to the waveguide is consistent with this interpretation[46]. The microelements were patterned by electron beam lithography (EBL) and consecutive ion beam etching. Following an initial oxygen plasma treatment for adhesive purposes, a negative resist (MA-N 2910) was spun onto the multilayer films. In a second step, the microelements were exposed by EBL. The samples were then developed for 300 s in MA-D 525 and rinsed in deionized water. Finally, the samples were exposed to an argon ion beam at two different angles (85° and 5°) to physically etch the magnetic microelements out of the continuous films. The remaining resist was removed by acetone and a second oxygen plasma treatment. For magnetic field excitation, a copper strip of 200 nm thickness was fabricated on top of the microelements by EBL, electron beam evaporation deposition and liftoff processing[54], resulting in a patterned microstrip 5 µm in width. The estimated Oersted field arising from a 1 mA electric current flowing through such a strip is about $\mu_0 H = 4\pi \times 10^{-2}$ mT.

Time-resolved STXM. Synchrotron STXM[52] was used to image the magnetic orientation in the multilayer microelements. Here, a monochromatic X-ray beam is focused onto the sample by means of a diffractive zone plate. The locally transmitted X-ray intensity is measured by a single-pixel detector, so raster scanning the sample provides a 2D absorption image of the sample with approximately 25 nm lateral resolution. Using circularly polarized X-rays allows XMCD[53] to be exploited, thus obtaining a magnetic contrast. As XMCD only occurs relevantly at the element-specific resonant absorption edges, the magnetic signal from both ferromagnetic layers, NiFe and CoFeB, can be separated by using X-rays of the corresponding L_3 energies, Ni L_3 ~853 eV and Co L_3 ~778 eV, respectively. On the other hand, a collective signal from both layers can be collected from the Fe L_3 edge at ~708 eV because both layers contain Fe. The acquired magnetic contrast scales with the projection of the magnetic orientation $\mathbf{m} = \mathbf{M}/M$ on the direction of photon propagation. Hence, in normal incidence, our STXM set-up is sensitive to the perpendicular magnetization component, while an inclined sample mounting also allows for detecting in-plane magnetization components at the same time.

Time-resolved STXM was used to stroboscopically image the magnetization dynamics of the multilayer microelements. This method utilizes the specific time structure of the incident X-rays, which comprises pulses with a 2 ns repetition rate and ~100 ps effective pulse length. Each incoming probe event (photon transmitted or not transmitted) is routed after every pulse to a periodic counting register of a field programmable gate array. Here, the number of registers (Q) sets the maximum non-stroboscopic observation period ($Q \times 2$ ns), while the number of excitation repetitions within this period sets the nominal time resolution as well as the excitation frequency in the case of a continuous sinusoidal excitation. The excitation current was monitored via −20 dB pick-off tees, both in front and behind the sample's signal line.

Theoretical model. We developed a theory for the calculation of spin wave dispersion relations in two extended interlayer exchange-coupled ferromagnetic layers.

The core of the theory is described in detail in the Supplementary Information. It considers spin wave modes in thin magnetic films, where the magnetization along the coordinate perpendicular to the film plane can be considered homogeneous. The case of thicker films, as in the experiment, is accounted for by splitting each ferromagnetic layer into a number N of thin films of equal thickness, so that for each of these films the thin film approximation holds. The N thin films of each layer are then coupled to each other by an effective ferromagnetic intralayer exchange coupling, whose strength is determined by estimating the energy of a magnetization distribution subject to homogeneous torsion and by requiring consistency with the continuum limit. The theory thus enables us to quickly compute dispersion relations for spin waves in the interlayer exchange-coupled bilayer system with ferromagnetic layers whose thicknesses exceed the exchange lengths of the respective material.

Micromagnetic simulations. Time integration of the Landau–Lifshitz–Gilbert[54,55] equation was carried out using the MuMax^3 code[56] for a spatially discretized, interacting lattice. The simulations were performed to compute the spin wave dispersion relations in the coupled layer system. The ferromagnetic layers are homogeneously magnetized and the dispersion relations are calculated in a thin film approach. Therefore, the system was discretized into (4096, 16, 115) (x,y,z) cells and periodic boundary conditions were applied along the y direction, which corresponds to the direction of equilibrium magnetization. The thickness of the individual layers and the spacer were chosen according to TEM measurements. This resulted in a cell size along the z axis of 0.8 nm. The material parameters used in the micromagnetic simulations are as follows. For NiFe, the respective values of saturation magnetization, exchange stiffness and uniaxial in-plane anisotropy are $M_s^{Py} = 800$ kA m^{-1}, $A_{xc}^{Py} = 7.5$ pJ m^{-1} (ref. [57]) and $K_u^{Py} = 200$ J m^{-3}. For the CoFeB layer, we used $M_s^{CoFeB} = 1{,}250$ kA m^{-1}, $A_{xc}^{CoFeB} = 12$ pJ m^{-1} (ref. [58]) and $K_u^{CoFeB} = 3{,}000$ J m^{-3}. The interlayer exchange coupling is $J = -0.1$ mJ m^{-2}. The Gilbert damping constants α for CoFeB and NiFe were chosen to be 0.008 and 0.01, respectively. To prevent reflection of spin waves from the edges, the damping was increased linearly to 0.065 for both layers.

An out-of-plane sinusoidal excitation field with a fixed frequency was applied in a 100-nm-wide region in the centre of the system. After the system reached dynamic equilibrium, the magnetization configuration was stored. To extract the wave number for each frequency a spatial fast-Fourier transform along the x direction of the system was performed. The corresponding dispersion relations are shown in Fig. 5 as grey full dots and are in good agreement with the results from the model calculations. Additional simulations were performed to compare the effects of oscillatory magnetic fields applied in-plane and out-of-plane, in each case perpendicular to the magnetization. The simulations clearly show that the bilayer system is more susceptible to out-of-plane field perturbations. This result can be understood taking into account the fact that the excited collective mode exhibits an in-phase oscillation of the perpendicular, yet anti-phase oscillation of the in-plane magnetization component (acoustic mode), and thus couples more efficiently to driving fields oriented perpendicular to the sample plane. There exists another type of collective mode in the system (optical mode), which exhibits an in-phase oscillation of the in-plane component; however, this mode resides at higher frequency values than the measured ones.

Due to the absence of domain walls, the thin film approach above cannot reproduce the observed 1D spin-wave dispersion within the walls and the emission of planar waves from them. To gain insight into these phenomena an elliptical bilayer with short and long axes of 2.16 µm and 3.24 µm, respectively, was simulated at a discretization of 648 × 432 × 115 cells. The material parameters were chosen to be the same as for the thin film approach, but for the slightly modified constants $A_{xc}^{Py} = 10.5$ pJ m^{-1}, $A_{xc}^{CoFeB} = 13$ pJ m^{-1}, $K_u^{CoFeB} = 5$ kJ m^{-3} and $J = -0.3$ mJ m^{-2}. To simulate the excitation of spin wave dynamics a spatially homogeneous sinc(t) pulse with a cutoff frequency of 10 GHz was utilized. To obtain the dynamic response the magnetization data was Fourier-transformed and filtered afterwards to extract the desired frequency.

Data availability

The data that support the plots within this paper and other findings of this study are available from the corresponding authors upon reasonable request.

References

51. Wintz, S. et al. Control of vortex pair states by post-deposition interlayer exchange coupling modification. *Phys. Rev. B* **85**, 134417 (2012).
52. Raabe, J. et al. PolLux: a new facility for soft X-ray spectromicroscopy at the Swiss Light Source. *Rev. Sci. Instrum.* **79**, 113704 (2008).
53. Schütz, G. et al. Absorption of circularly polarized X rays in iron. *Phys. Rev. Lett.* **58**, 737–740 (1987).
54. Landau, L. & Lifshits, E. On the theory of the dispersion of magnetic permeability in ferromgnetic bodies. *Phys. Z. Sow.* **8**, 135 (1935).
55. Gilbert, T. L. A Lagrangian formulation of the gyromagnetic equation of the magnetization field. *Phys. Rev.* **100**, 1243 (1955).
56. Vansteenkiste, A. et al. The design and verification of MuMax3. *AIP Adv.* **4**, 107133 (2014).
57. Wei, J. et al. Annealing influence on the exchange stiffness constant of permalloy films with stripe domains. *J. Phys. D* **49**, 265002 (2016).
58. Conca, A. et al. Annealing influence on the Gilbert damping parameter and the exchange constant of CoFeB films. *Appl. Phys. Lett.* **104**, 182407 (2014).